

RESEARCH

Open Access



# Vitamin A mediates FABP4 to regulate intramuscular fat production: a new target and strategy for optimizing beef quality

Yaping Song<sup>1,2†</sup>, Jiupan Zhang<sup>3†</sup>, Chao Jiang<sup>1,2</sup>, Xiaoyu Song<sup>1,2</sup>, Xiaodong Chen<sup>1,2</sup>, Sayed Haidar Abbas Raza<sup>4</sup>, Sameer Dinkar Pant<sup>5</sup>, Yun Ma<sup>1,2</sup>, Linsen Zan<sup>6</sup>, Dawei Wei<sup>1,2\*</sup> and Guijie Zhang<sup>1,2\*</sup>

## Abstract

Beef quality is critically determined by intramuscular fat (IMF) deposition. Retinoic acid (RA), the active metabolite of vitamin A, plays an essential regulatory role in IMF development. To systematically investigate RA-mediated regulation of IMF formation in cattle, we established a concentration gradient of RA supplementation and employed a systematic screening approach to identify the optimal dosage for modulating bovine intramuscular adipocytes (IMAs) proliferation and differentiation. Subsequently, leveraging integrated multi-omics approaches, we screened the key downstream molecular targets through which RA governs IMF biosynthesis, and clarified the potential regulatory mechanism of this target. Our experimental data establish that RA promotes the proliferation of IMAs through modulation of G1/S phase progression. Concurrently, RA enhances triglyceride biosynthesis in IMAs by activating PPAR $\gamma$ -mediated cell differentiation and LPL-mediated intracellular lipid accumulation. Integrated transcriptomics and metabolomics analyses identified *FABP4*, *CD36*, *EBF2*, *LRP1* and *CAV1* as key candidate genes involved in RA-mediated IMF production. Functional interrogation revealed that *FABP4* knockdown markedly attenuated lipid accumulation in IMAs, a phenotype rescued through RA supplementation, confirming *FABP4* as the critical effector mediating vitamin A's regulation of bovine IMF deposition. These results provide a new understanding of how nutritional factors affect beef quality at the molecular level.

**Keywords** Bovine, Intramuscular fat, Vitamin A, FABP4

<sup>†</sup>Yaping Song and Jiupan Zhang contributed equally to this work.

\*Correspondence:

Dawei Wei

weidawei@nxu.edu.cn

Guijie Zhang

guijiezh@nxu.edu.cn

<sup>1</sup>College of Animal Science and Technology, Ningxia University, Yinchuan 750021, China

<sup>2</sup>Key Laboratory of Ruminant Molecular Cell Breeding, Ningxia Hui Autonomous Region, Yinchuan 750021, China

<sup>3</sup>Institute of Animal Science, Ningxia Academy of Agriculture and Forestry Sciences, Yinchuan 750021, China

<sup>4</sup>State Key Laboratory of Biocontrol, School of Life Sciences, Sun Yat-Sen University, Guangzhou, Guangdong 510006, China

<sup>5</sup>Gulbali Institute, Charles Sturt University, Wagga Wagga, NSW 2678, Australia

<sup>6</sup>College of Animal Science and Technology, Northwest A&F University, Yangling 712100, China



## Introduction

Beef serves as a globally consumed nutrient-rich food prized for its characteristic flavor profile, provides abundant high-quality protein, essential amino acids, micro-nutrients, and vitamins [1, 2]. The persistent domestic supply-demand imbalance for premium-grade beef has established genetic optimization of meat quality attributes as a strategic priority in modern bovine breeding programs [3]. IMF content, a primary determinant of beef palatability and nutritional value [4], arises through precisely regulated preadipocytes proliferation and terminal differentiation into lipid-accumulating mature adipocytes [5, 6]. Systematic elucidation of molecular regulation mechanisms governing IMAs development thus constitutes an essential foundation for enhancing beef quality via genetic improvement strategies.

Vitamin A and related dietary nutrients critically regulate IMF (marbling) deposition in cattle [7]. As an essential liposoluble micronutrient obtained by ruminants through dietary sources, including plant-based diets, vitamin premix or feed additives containing precursor forms (e.g. beta-carotene) [4, 8]. Vitamin A exhibits paradoxical regulatory effects across developmental stages. Previous research indicates that injecting vitamin A into newborn calves could increase fat progenitor cells in skeletal muscle, thus improving growth performance and marbling potential [9, 10]. Conversely, vitamin A could inhibit IMAs differentiation and maturation in adult cattle through RA and its derivatives, consequently suppressing IMF deposition [11]. As the principal bioactive metabolite of vitamin A [12], RA biosynthesis involves sequential enzymatic oxidation catalyzed by alcohol dehydrogenase and aldehyde dehydrogenase [13]. *In vivo*, vitamin A mainly performs its physiological role through RA [4], which operates by binding to the retinoic acid receptor (RAR) and retinoic acid X receptor (RXR) [14]. Current evidence reveals that RA has varying effects on adipocyte development, it can either enhance preadipocyte proliferation and differentiation or inhibit 3T3-L1 cell differentiation at low concentrations ( $1 \times 10^{-5}$  mol/L or  $5 \times 10^{-6}$  mol/L) [15, 16]. Despite these mechanistic insights, the molecular circuitry governing RA-mediated adipocyte regulation in bovine systems remains insufficiently characterized. Existing investigations have predominantly focused on phenotypic outcomes, with limited exploration of RA-associated transcriptional networks and epigenetic modifiers. Elucidating the RA-regulated molecular landscape of lipid accumulation could enable identification of targeted intervention strategies. Such advancements would facilitate precision enhancement of meat quality parameters and marbling characteristics while maintaining rigorous animal welfare standards.

Therefore, this study systematically delineates dose-dependent effects of RA on bovine IMAs proliferation and differentiation, identifying optimal regulatory concentration for adipogenesis modulation. Integrated transcriptomic and metabolomic profiling revealed *FABP4* as a pivotal mediator of RA-regulated the lipid accumulation in IMAs, with functional validation confirming its regulatory dominance. Mechanistic analyses elucidated RA-*FABP4* signaling axis coordination in controlling intramuscular lipogenesis and lipid droplet maturation, establishing a molecular framework for precision modulation of IMF deposition. These findings provide actionable insights for strategic development of genetic selection markers and nutritional interventions targeting marbling enhancement in beef production systems.

## Methods

### Ethics and consent to participate

The animal experiments were conducted in strict accordance with the ethical guidelines established by the Chinese Association for Laboratory Animal Sciences, with experimental protocols receiving prior approval from the Animal Ethics Committee at Ningxia University (NXU-2023-108). All experimental animals used have obtained the informed consent of their owners, and there are no conflicts of interest.

### Sample collection

IMAs isolation specimens were obtained from the longissimus dorsi muscle of six neonatal (one-week-old) Guyuan yellow cattle, selected from distinct genetic lineages within the breeding population of the Fu Min Agricultural Science and Technology Co., Ltd. (Ningxia, China). All procedures were conducted in accordance with institutional animal care protocols, with euthanasia performed via intravenous administration of pentobarbital sodium (80 mg/kg) following established welfare guidelines. The samples were aseptically collected, thoroughly rinsed with a 75% alcohol solution followed by Phosphate Buffered Saline solution (PBS; Hyclone, Logan, Utah, USA) to minimize contamination, before being immediately transported to the cell culture laboratory.

### Isolation, culture, and differentiation of IMAs

IMAs were isolated according to the established enzymatic digestion protocol [17]. Briefly, longissimus dorsi muscle samples were aseptically cut into approximately 1 mm<sup>3</sup> pieces and subjected to digestion with collagenase type II (Solarbio, Beijing, China). Sequential filtration through 40 μm and 70 μm cell sieves in turn to remove impurities, followed by centrifugation (1,000 rpm, 10 min) to pellet viable cells. Pellet resuspension in Dulbecco's Modified Eagle Medium/high glucose (DMEM/high glucose) medium (Hyclone) and differential

adhesion was employed to reduce impurities. IMAs differentiation was induced at 100% confluence using differentiation medium containing DMEM/high glucose supplemented with 0.5 mmol/L isobutylmethylxanthine (IBMX), 10 µg/mL insulin, 1 µmol/L rosiglitazone, and 1 µmol/L dexamethasone, all sourced from Sigma. After 48 h induction, cultures were maintained in DMEM/high glucose with insulin and rosiglitazone [18]. In addition, phenotype identification (lipid droplets staining), immunofluorescence staining (PPAR $\gamma$ ) and marker genes expression profile identification (PPAR $\gamma$  and *C/EBP $\alpha$* ) were used to identify the purity and differentiation potential of purified IMAs. Following rigorous purification and characterization, the third generation of IMAs were utilized in a series of subsequent experiments.

#### Lipid droplets staining

IMAs ( $n=3$ ) were seeded in 6-well culture plates at a density of  $1 \times 10^4$  cells/well, achieving uniform monolayer confluence prior to differentiation induction. Cells were treated with RA (Solarbio) at six concentrations ( $0$ ,  $10^{-9}$ ,  $10^{-8}$ ,  $10^{-7}$ ,  $10^{-6}$  and  $10^{-5}$  mol/L), dissolved in 0.1% DMSO (v/v). On day 6 of differentiation, cells were fixed with 4% paraformaldehyde for 1 h and subsequently washed with PBS. Cells were stained for 20 min using either Bodipy (5 µM; Amgicam, Wuhan, China), Nile red (1 µg/mL; Amgicam) or oil red O (3 µg/mL; Solarbio) working solutions. Cells stained with oil red O were counterstained with hematoxylin (1 mg/mL; Solarbio) for 2 min, while those stained with Bodipy or Nile red were counterstained with DAPI (5 µg/mL; Solarbio) for 10 min. All stained cells were examined using inverted fluorescent microscope (OLYMPUS, Tokyo, Japan).

#### Immunofluorescence staining

The IMAs ( $n=3$ ) were inoculated into 24-well plates ( $2.5 \times 10^3$  per well). Upon reaching approximately 80% confluence, cells were fixed with 4% paraformaldehyde (30 min) and permeabilized with 0.3% Triton X-100 (15 min). Following blocking with 5% BSA (Solarbio), samples were incubated overnight with PPAR $\gamma$  antibody (1: 100) at 4°C. After washing, the secondary antibodies (1: 500) were incubated for 1 h in the dark at room temperature, followed by stained with DAPI for 10 min. Specimens underwent three PBS washes before imaging on an inverted microscope. Antibody information in Supplementary Table S1.

#### Total RNA extraction and real-time quantitative PCR (RT-qPCR)

Total RNA extraction and cDNA synthesis were performed using the Takara's kit (Takara Bio, Shiga, Japan) [18]. RT-qPCR was conducted using the  $2 \times$  M5 HiPer SYBR Premix EsTaq Fluorescence Quantitative PCR

Kit (Mei5bio, Beijing, China) on a Bio-Rad CFX96 Real-Time PCR Detection System (California, USA). Glyceraldehyde-3-phosphate dehydrogenase (*GAPDH*) served as the endogenous control for normalization [19], with relative gene expression quantified via the  $2^{-\Delta\Delta C_t}$  method [20]. Primers information were shown in Supplementary Table S2.

#### EdU staining

IMAs ( $n=3$ ) were seeded onto 24-well plates ( $2.5 \times 10^3$  per well) and treated with varying concentrations of RA. After 48 h, cells were incubated with 20 µM EdU (Beyotime, Shanghai, China) at 37 °C for 1 h. Post-incubation, cells were fixed with 4% paraformaldehyde (30 min) and membrane permeabilized using 0.3% Triton X-100 (15 min). After washing, cells were incubated with Click reaction solution in the dark (30 min), followed by nuclei counterstaining with Hoechst33342 solution (Beyotime) for 10 min. Fluorescent imaging was performed on an inverted fluorescent microscope.

#### Cell cycle detection

IMAs ( $n=3$ ) were enzymatically detached using 0.25% trypsin and collected in 1.5 mL Eppendorf (EP) tubes. Cells were fixed in 70% ethanol at 4 °C for 12 h, then stained with propidium iodide and incubated in the dark at 37 °C for 30 min. Finally, the cell cycle was analyzed by flow cytometry (BD Bio sciences, New Jersey, USA).

#### Western blot (WB)

Total protein extraction from IMAs ( $n=3$ ) was performed using the kit of KeyGEN (Jiangsu, China). Aliquots (10 µg per channel) underwent electrophoretic separation on 10% SDS-PAGE gels (200 V, 30 min) followed by transfer to PVDF membrane (Millipore Corporation, USA). The membrane was blocked with fast protein blocking solution (Yazyme Biotechnology Shanghai; China) for 15 min at room temperature prior to overnight incubation with primary antibody (4 °C; dilutions in Supplementary Table S1) Following three TBST washes (10 min each), membranes were incubated with secondary antibody for 2 h at room temperature. Chemiluminescent detection was performed using the Tanon-5200 imaging system (Tanon, Shanghai, China).

#### Determination of triglyceride (TG)

IMAs ( $n=3$ ) were harvested at differentiation day 6 and pelleted in 1.5 mL centrifuge tubes. Subsequently, cell pellets were homogenized in 200 µL buffer by ultrasonic disruption. Cellular TG content were measured using a triglyceride determination kit (Nanjing Chengjian Institute of Bioengineering, Nanjing, China).

### RNA-seq and UHPLC-MS/MS analysis

IMAs were seeded onto 6-well plates ( $1 \times 10^4$  per well) and differentiated at full confluence. Cells were treated with either 0 mol/L or  $10^{-5}$  mol/L RA. On the sixth day of differentiation, total RNA ( $n=3$ ) was extracted and sequenced on an Illumina NovaSeq 6000 platform (Denovo Biotechnology, Guangzhou, China). Differentially expressed genes (DEGs) were identified using thresholds of  $P \leq 0.05$  and a fold change greater than 1.5 [3]. A randomly selected subset of DEGs underwent technical validation via RT-qPCR (primers sequences in Supplementary Table S2). Under identical treatment conditions, cellular metabolites ( $n=6$ ) were analyzed using LC-MS/MS (1290 Infinity LC, Agilent Technologies) [18]. Differentially expressed metabolites (DEMs) were identified using thresholds of  $VIP > 1$  and  $P \leq 0.05$ . To clarify how RA influences fat formation, an integrated analysis of transcriptomic and metabolomic data was conducted. This involved the construction of pathway function models, O2PLS models and correlation coefficient models using gene expression and metabolite abundance data [18].

### Synthesis and transfection of small interfering RNA targeting bovine *FABP4* (si-*FABP4*)

The si-*FABP4* and a negative control (NC) were synthesized (Table S3). IMAs were seeded onto 6-well plates at a density of 10,000 cells per well. Upon reaching 80% confluence, the medium was replaced with Opti-MEM™ (Invitrogen) and transfected with si-*FABP4* or NC using Lipofectamine 3000 reagent (Invitrogen). Following 6-hour transfection, medium was replaced with adipogenic induction cocktail containing either 0 (NC) or  $10^{-5}$  mol/L RA for experimental groups (NC+RA, si-*FABP4*+RA).

### Data analysis and statistics

Cell proliferation rates were determined using ImageJ software (Bethesda, Maryland, USA) by calculating the ratio of EdU-positive cells to total nuclei. FlowJo\_v 10.6.2 software (BD Biosciences) was utilized to analyze the cell cycle. The relative expression of lipid droplets was quantified using Image Pro Plus software (MEDIA CYBERNETICS, Maryland, USA). Significance was assessed via a t-test using GraphPad Prism 8.0 (San Diego, CA, USA), \*\* denotes a highly significant difference ( $P < 0.01$ ), and \* denotes a significant difference ( $P < 0.05$ ). Principal Component Analysis (PCA) was performed using R (<http://www.r-project.org/>). DEGs between two groups of samples was analyzed by DESeq2. Additionally, DEGs were comprehensively associated with the Gene Ontology (GO) database (<http://www.geneontology.org/>), and the quantity of DEGs within each functional category was systematically enumerated. Using hypergeometric

test strategy, KEGG pathway is used as the basic unit to identify the signal pathways enriched by DEGs. With the help of Ropl software package in R, OPLS-DA analysis is carried out. DEMs between comparison groups were identified by integrating the VIP value from OPLS-DA with multivariate statistical analysis and the  $P$  value from a univariate  $t$ -test. The enrichment of pathways identifies key biochemical and signal transduction pathways involving DEMs.

## Results

### Isolation and identification of bovine IMAs

In this study, IMAs were successfully isolated by enzyme digestion, with the obtained cells displaying robust viability, uniform morphology, and characteristic elongated spindle-shape features (Fig. 1A). Lipid droplets accumulation became evident by differentiation day 8 through oil red O staining, manifested as distinct bright red spherical formations (Fig. 1B). Bodipy staining further confirmed the high lipid content of IMAs, indicated by intense fluorescence (Fig. 1C). Immunofluorescence staining detected strong expression of the adipogenic marker PPAR $\gamma$  (Fig. 1D). Additionally, RT-qPCR analysis demonstrated that compared with the 0th day, PPAR $\gamma$  and *C/EBP $\alpha$*  were significantly up-regulated during the differentiation of IMAs (Fig. 1E-F). These findings demonstrate that the isolated IMAs are highly pure and capable of differentiation.

### Vitamin A influences the proliferation of IMAs

To assess the effect of Vitamin A on IMAs proliferation, cells were treated with RA at concentrations ranging from 0 to  $10^{-5}$  mol/L. EdU staining revealed reduced proliferation at  $10^{-8}$  mol/L RA compared to untreated control (0 mol/L RA), whereas  $10^{-7}$  and  $10^{-5}$  mol/L RA significantly enhanced proliferation activity ( $P < 0.05$  and  $P < 0.01$ , respectively; Fig. 2A-B). Flow cytometry analysis revealed that  $10^{-8}$  mol/L RA significantly elevated the percentage of cells in the G1 phase ( $P < 0.01$ , Fig. 2C-I), while  $10^{-5}$  mol/L RA reduced the percentage of cells in the G1 phase and elevated the percentage in the S phase ( $P < 0.05$ , Fig. 2I). RT-qPCR results demonstrated that  $10^{-8}$  mol/L RA suppressed *PCNA* and *CDK1* expression ( $P < 0.01$ ), whereas higher concentrations RA ( $10^{-7}$  ~  $10^{-5}$  mol/L) induced pronounced upregulation of *PCNA* ( $P < 0.01$ , Fig. 2J). *CDK1* expression increased significantly at  $10^{-9}$ ,  $10^{-7}$  and  $10^{-5}$  mol/L RA ( $P < 0.01$ , Fig. 2K), while *CDK2* expression were elevated at  $10^{-9}$ ,  $10^{-8}$  and  $10^{-5}$  mol/L RA ( $P < 0.05$ , Fig. 2L). The results of WB confirmed elevated that *PCNA* and *CDK2* protein expression levels following  $10^{-5}$  mol/L RA exposure ( $P < 0.01$ , Fig. 2M, Fig. S1). Collectively, these findings suggest that  $10^{-8}$  mol/L RA inhibits IMAs proliferation by impeding G1/S phase transition, whereas  $10^{-5}$  mol/L RA promotes

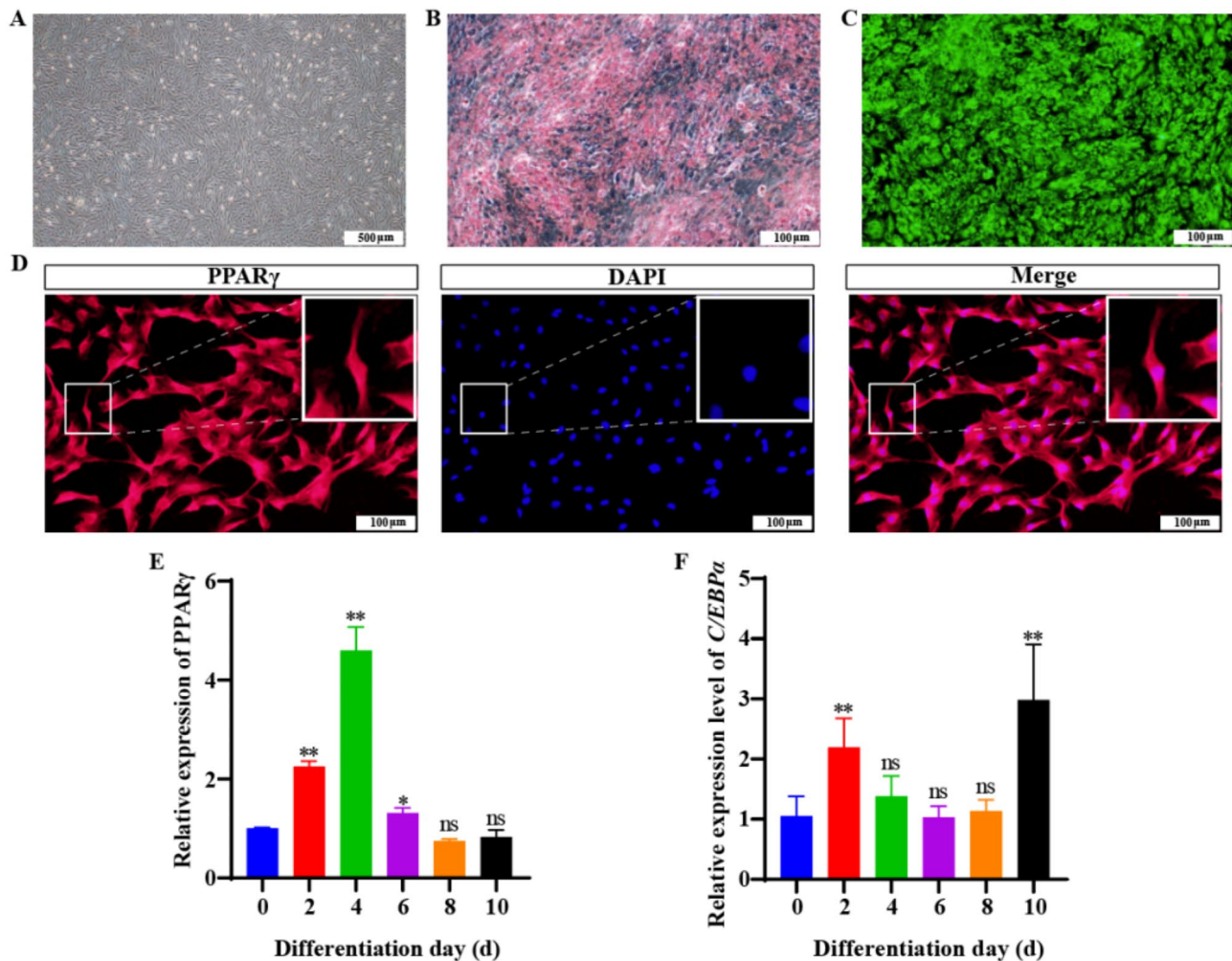


**Fig. 1** Morphological and molecular characterization of IMAs. (A) Representative image of IMAs at 100% confluence; (B) Oil Red O staining of IMAs on 8th day of differentiation; (C) Bodipy staining of IMAs on 8th day of differentiation; (D) Immunofluorescence staining for PPAR $\gamma$ ; (E-F) The mRNA expression levels of adipogenic markers PPAR $\gamma$  and C/EBP $\alpha$  were analyzed in IMAs at different differentiation stages (0, 2, 4, 6, 8, and 10 days)

IMAs proliferation through transcriptional upregulation of *PCNA*, *CDK1* and *CDK2*, accelerating cell cycle progression.

#### Vitamin A enhances the differentiation and lipid metabolism of IMAs

To investigate the regulatory role of vitamin A in IMAs differentiation and lipid metabolism, cells were treated with RA across a concentration gradient ( $10^{-9}$  to  $10^{-5}$  mol/L). Phenotypic analysis revealed that RA-induced dose-dependent lipid droplets accumulation and elevated TG levels in all treatment groups (Fig. 3A-C). Additionally, the expression of key lipogenic marker genes, including PPAR $\gamma$  and *LPL*, was upregulated in IMAs upon RA treatment (Fig. 3D-E, Fig. S1). The findings indicate that RA concentrations between  $10^{-9}$  mol/L to  $10^{-5}$  mol/L enhance IMAs differentiation and lipid metabolism, with the highest lipid accumulation at  $10^{-5}$  mol/L RA.

#### Screening of DEGs and its functional analysis

To further elucidate the molecular mechanism underlying Vitamin A-mediated IMF formation, IMAs were treated with the optimal RA concentration ( $10^{-5}$  mol/L). PCA analysis (Fig. 4A) and sample correlation heatmap analysis (Fig. 4B) confirmed the reproducibility of the samples. RNA-seq revealed 344 DEGs in the RA-treated group compared to the control group, with 171 DEGs up-regulated and 173 down-regulated (Fig. 4C-D). RNA-seq reliability was corroborated by RT-qPCR, which showed consistent expression patterns for selected genes (Fig. 4E). Among the screened DEGs, 17 genes were closely related to lipogenesis, including *FABP4*, *CD36*, *ELOVL2* and *FADS2B* (Fig. 4C and F). PPI network analysis revealed that *FABP4* directly interacted with *CD36* and *ELOVL2* (Fig. 4G). GO enrichment analysis revealed significant enrichment of DEGs in biological processes associated with fat formation, including fatty acid metabolic process (GO:0006631), unsaturated fatty

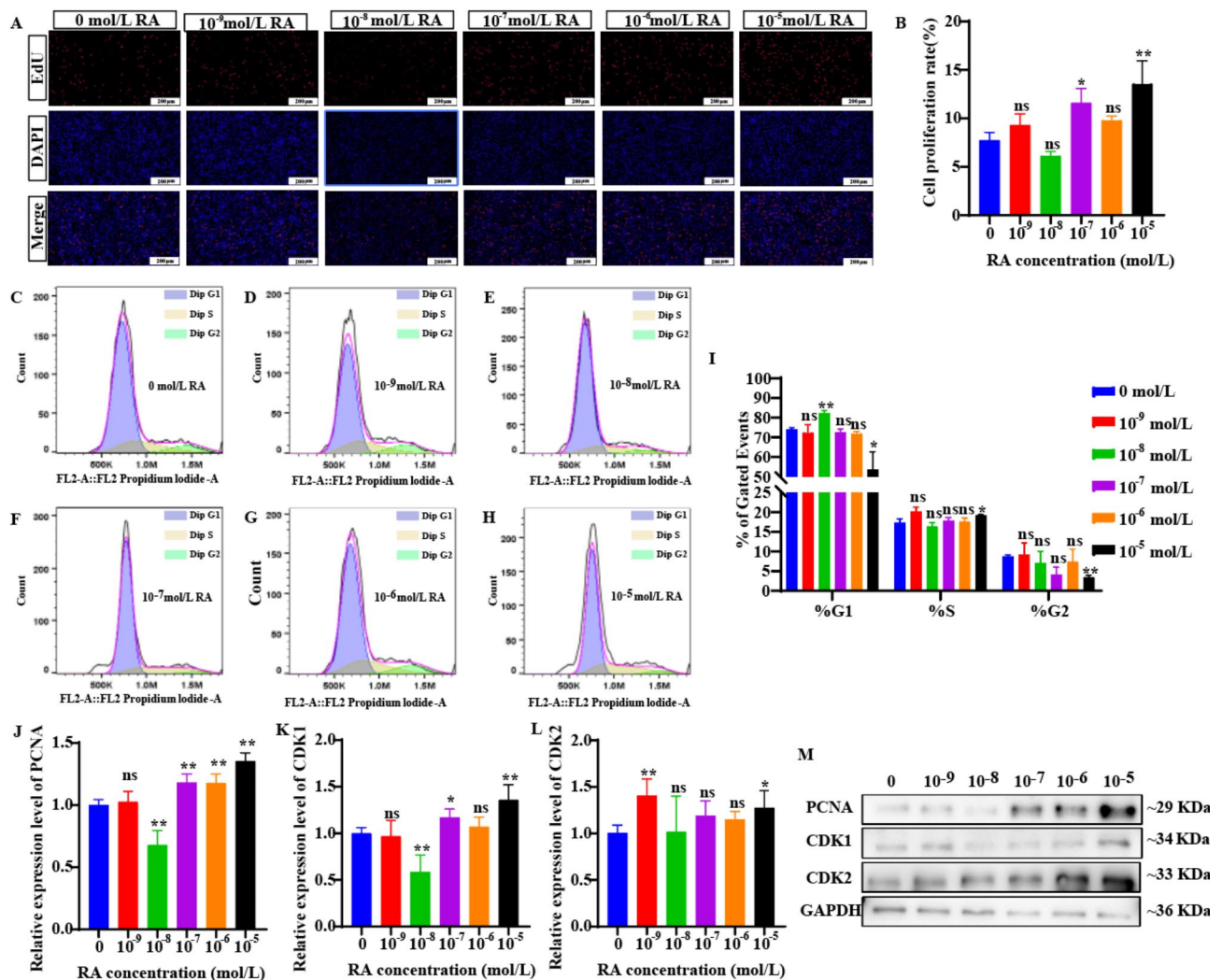


**Fig. 2** The regulatory effect of different concentrations of RA on the proliferation of IMAs. **(A)** Representative images show EdU (red) and Hoechst 33,342 (blue) staining in IMAs exposed to RA concentrations of 0,  $10^{-9}$ ,  $10^{-8}$ ,  $10^{-7}$ ,  $10^{-6}$  and  $10^{-5}$  mol/L RA; **(B)** Quantification of EdU-positive cells; **(C-H)** Representative flow cytometry plots of cell cycle distribution in IMAs treated with different concentrations of RA; **(I)** Quantification of the cell percentage in G1, S and G2 phases; **(J-L)** Relative mRNA expression of *PCNA*, *CDK1* and *CDK2* in IMAs treated with different concentrations of RA; **(M)** Representative western blots and quantification of *PCNA*, *CDK1* and *CDK2* protein expression in IMAs treated with different concentrations of RA

acid metabolic process (GO:0033559) and fat cell differentiation (GO:0045444) ( $P < 0.05$ , Fig. 4H). Furthermore, KEGG enrichment analysis revealed that the DEGs were significantly associated with adipogenesis-related pathways, including adipocytes lipolysis regulation (ko04923), PPAR signaling pathway (ko03320), and calcium signaling pathway (ko04020) ( $P < 0.05$ , Fig. 4I).

**Screening for DEMs and its functional analysis**

Non-targeted metabolomic profiling of RA-treated IMAs was performed to investigate the mechanism vitamin A-mediated metabolites in the regulation of IMF formation. Multivariate statistical analysis, including OPLS-DA, validated model robustness (Fig. S2). Differential expression analysis identified 262 DEMs, with 128 in POS mode (91 up-regulated and 37 down-regulated)

and 134 in NEG mode (32 up-regulated and 102 down-regulated) (Fig. 5A-C). Heatmap visualization highlighted 17 metabolites exhibiting significant associations with lipogenesis, including M285T85\_NEG (Androstendione), M465T28\_2\_NEG (Cholesteryl sulfate), M349T27\_2\_NEG (Tetrahydrocorticosterone), M362T126\_1\_POS (D-erythro-sphingosine-1-phosphate), M302T66\_POS (Pro-Trp), M444T38\_POS (Psychosine), and others DEMs ( $P < 0.05$ , Fig. 5D-E). KEGG pathway enrichment analysis of POS mode DEMs revealed significant enrichment in adipogenesis-associated pathways, including sphingolipid metabolism (ko00600), glycerophospholipid metabolism (ko00564), steroid hormone biosynthesis (ko00140) and fatty acid metabolism (ko01212) (Fig. 5F). NEG mode DEMs predominantly mapped to steroid hormone biosynthesis (ko00140), biosynthesis of

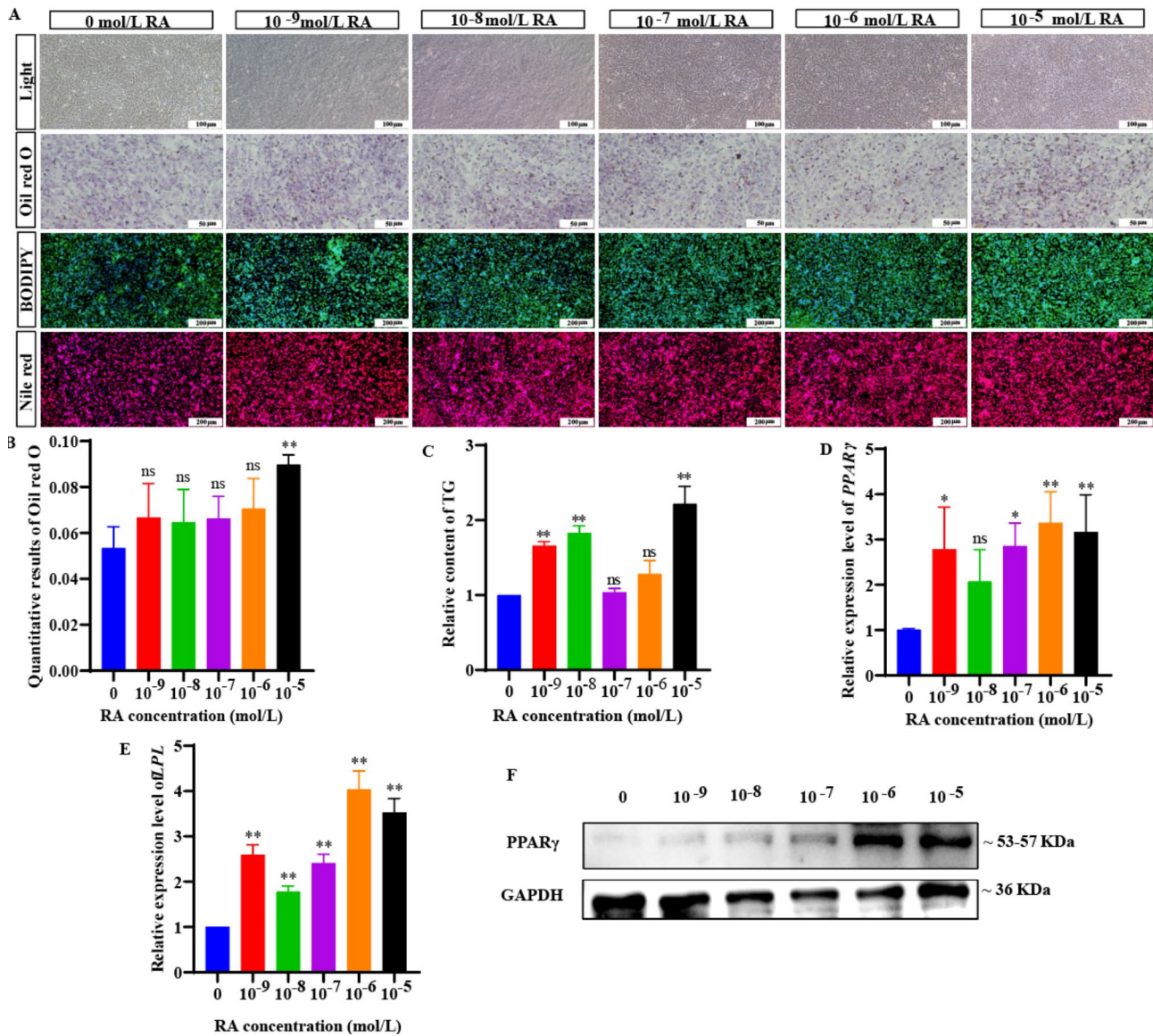


**Fig. 3** The regulatory effect of different concentrations of RA on the differentiation of IMAs. **(A)** Representative images of IMAs stained with oil red O, Bodipy, and Nile red after treatment with RA at concentrations of 0, 10<sup>-9</sup>, 10<sup>-8</sup>, 10<sup>-7</sup>, 10<sup>-6</sup> and 10<sup>-5</sup> mol/L RA; **(B)** Quantification of oil red O staining intensity; **(C)** TG content in IMAs across different RA concentrations; **(D-E)** mRNA expression levels of *PPARγ* and *LPL* in IMAs treated with varying RA concentrations; **(F)** Protein expression levels of *PPARγ* in IMAs with different RA concentrations

unsaturated fatty acids (ko01040), and fatty acid biosynthesis (ko00061) (Fig. 5G). These findings suggested that vitamin A modulates multiple metabolic pathways to regulate IMF formation.

**Integrated analysis of transcriptomic and metabolomic data**

To further identify key DEGs and metabolites influencing adipogenesis, three analytical model were employed to jointly analyze transcriptomic and metabolomic data. Cross-omics analysis revealed co-enriched of DEGs and DEMs in multiple adipogenesis-related pathways, including the calcium signaling pathway (ko04020),

biosynthesis of unsaturated fatty acids (ko01040), insulin resistance (ko04931), fatty acid metabolism (ko01212), glycerophospholipid metabolism (ko00564), and steroid hormone biosynthesis (ko00140)(Table S4). The top 10 DEMs and DEGs with significant loading values were presented in Fig. 6A. Multivariate integration of DEGs and DEMs, weighted by squared loading values, identified 25 hub features for network mapping. This analysis demonstrated strong associations between metabolites (e.g., M532T30\_POS, M891T348\_NEG, acetildenafil) and adipogenesis-linked genes, with PTPRN2, EBF2, and KIAA2012 exhibiting the strongest correlations. Notably, EBF2 emerged as a pivotal transcriptional regulator of

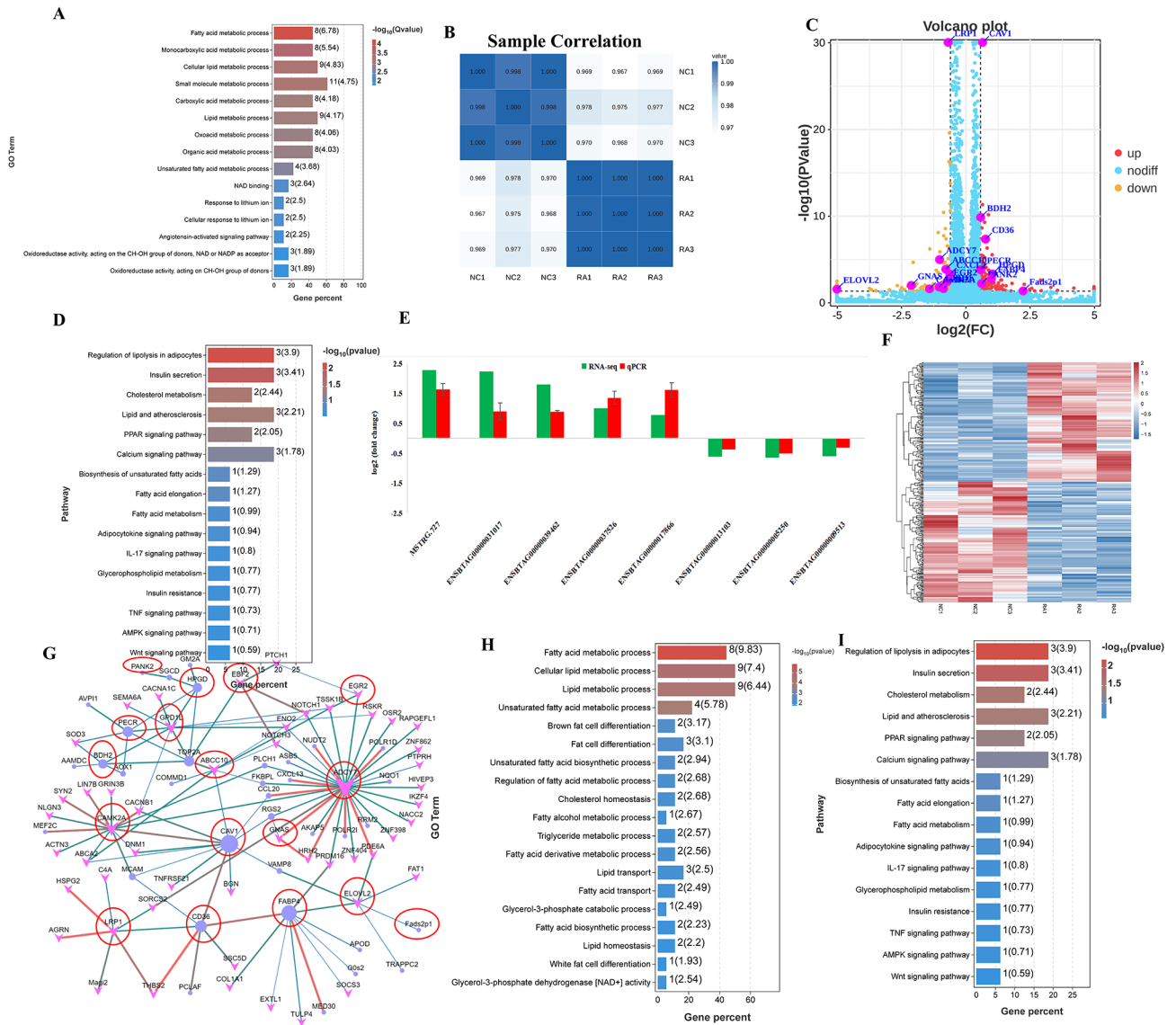


**Fig. 4** Identification and Functional Analysis of DEGs. **(A)** PCA visualization. The horizontal axis denotes the first principal component (PC1), while the vertical axis denotes the second principal component (PC2); **(B)** Sample correlation heatmap displays pairwise Pearson correlation coefficients among samples. Color intensity indicates correlation strength, with darker shades showing higher correlation; **(C)** Volcano plot illustrating DEGs. Red dots indicate upregulated DEGs, yellow dots indicate down-regulated DEGs, and blue dots indicate non-significant genes; **(D)** Histogram showing the distribution of DEGs, detailing the count of upregulated and down-regulated genes; **(E)** RT-qPCR validation of RNA-seq findings; **(F)** Heatmap depicting DEG expression patterns across samples; **(G)** PPI network for DEGs, emphasizing potential functional interactions among encoded proteins. The red circle highlights the close relationship between DEGs and lipogenesis; **(H)** GO enrichment analysis identifies DEGs linked to adipogenesis; **(I)** KEGG pathway enrichment analysis of DEGs is conducted. The x-axis displays the gene ratio, while the y-axis shows enriched pathways. Bar size reflects the gene count, and bar color denotes the significance of enrichment

adipogenic differentiation (Fig. 6B, Supplementary Table S5).

Furthermore, heatmap and network diagram analyses identified significant correlations between adipogenesis-associated genes and metabolites ( $P < 0.05$ , Table S6, Fig. 6C-D). Specifically, the adipogenic marker *FABP4* (ENSBTAG00000037526) was significantly correlated with M362T126\_1\_POS (D-erythro-sphingosine-1-phosphate) and M400T78\_POS (L-palmitoylcarnitine). The

*CD36* (ENSBTAG00000017866) was significantly associated with M444T38\_POS (4-androsten-17 $\beta$ -ol-3-one glucosiduronate), M362T126\_1\_POS (D-erythro-sphingosine-1-phosphate), M465T462\_POS (4-androsten-17 $\beta$ -ol-3-one glucosiduronate), M400T78\_POS (L-palmitoylcarnitine) and M465T28\_2\_NEG (Cholesteryl sulfate). Similarly, *LRP1* (ENSBTAG00000010830) was significantly associated with M444T38\_POS (4-androsten-17 $\beta$ -ol-3-one glucosiduronate),

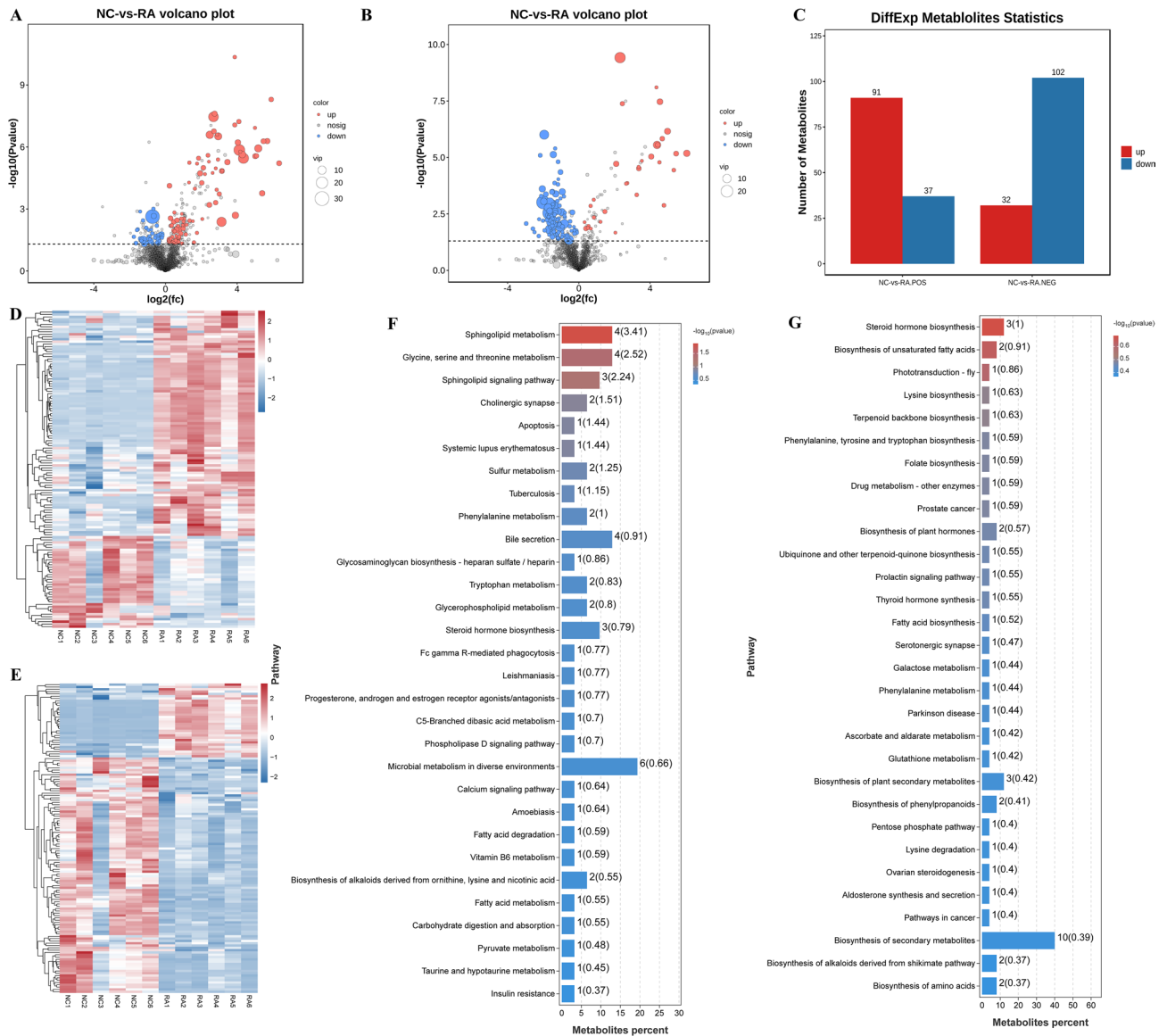


**Fig. 5** Screening for DEMs and its functional analysis. **(A)** Volcano plot depicting DEMs in positive (POS) ion mode. Red dots indicate upregulated DEMs, yellow dots signify downregulated DEMs ( $FC < -1$ ,  $VIP \geq 1$  and  $P < 0.05$ ), and blue dots denote metabolites that do not meet the significance criteria; **(B)** Volcano plot depicting DEMs in negative (NEG) ion mode; **(C)** Quantitative analysis of DEMs; **(D)** Heatmap of hierarchical clustering of DEMs in POS mode. The dataset comprises rows for metabolites and columns for samples, with metabolite abundance normalized using z-scores. Red signifies greater abundance, while blue denotes lesser abundance. Metabolites and samples are clustered based on their abundance profiles; **(E)** Heatmap of hierarchical clustering of DEMs in NEG mode; **(F)** KEGG pathway enrichment analysis of DEMs in the POS mode. The plot illustrates the top 30 KEGG pathways enriched for DEMs in POS mode, ranked by  $p$ -value. **(G)** KEGG pathway enrichment analysis of DEMs in the NEG mode

M362T126\_1\_POS (D-erythro-sphingosine-1-phosphate) and M465T28\_2\_NEG (Cholesteryl sulfate). *CAVI* (ENSBTAG00000017869) was also significantly associated with M444T38\_POS (4-androsten-17 $\beta$ -ol-3-one glucosiduronate), M362T126\_1\_POS (D-erythro-sphingosine-1-phosphate) and M465T28\_2\_NEG (Cholesteryl sulfate). Integrative multi-model analysis prioritized *FABP4*, *CD36*, *EBF2*, *LRP1* and *CAVI* as central mediators of vitamin A's adipogenic regulation.

**FABP4 functions as a primary target gene of RA in mediating IMF formation regulation**

To identify molecular targets mediating vitamin A's regulation of IMF formation in cattle, transcriptomic and metabolomic datasets were integrated through interaction network analysis. A coordinated regulatory axis emerged between lipogenesis-associated DEGs and DEMs, revealing a multi-layered network governing adipogenic processes (Fig. 7A). Network analysis identified *FABP4* as a central hub, functionally linked to

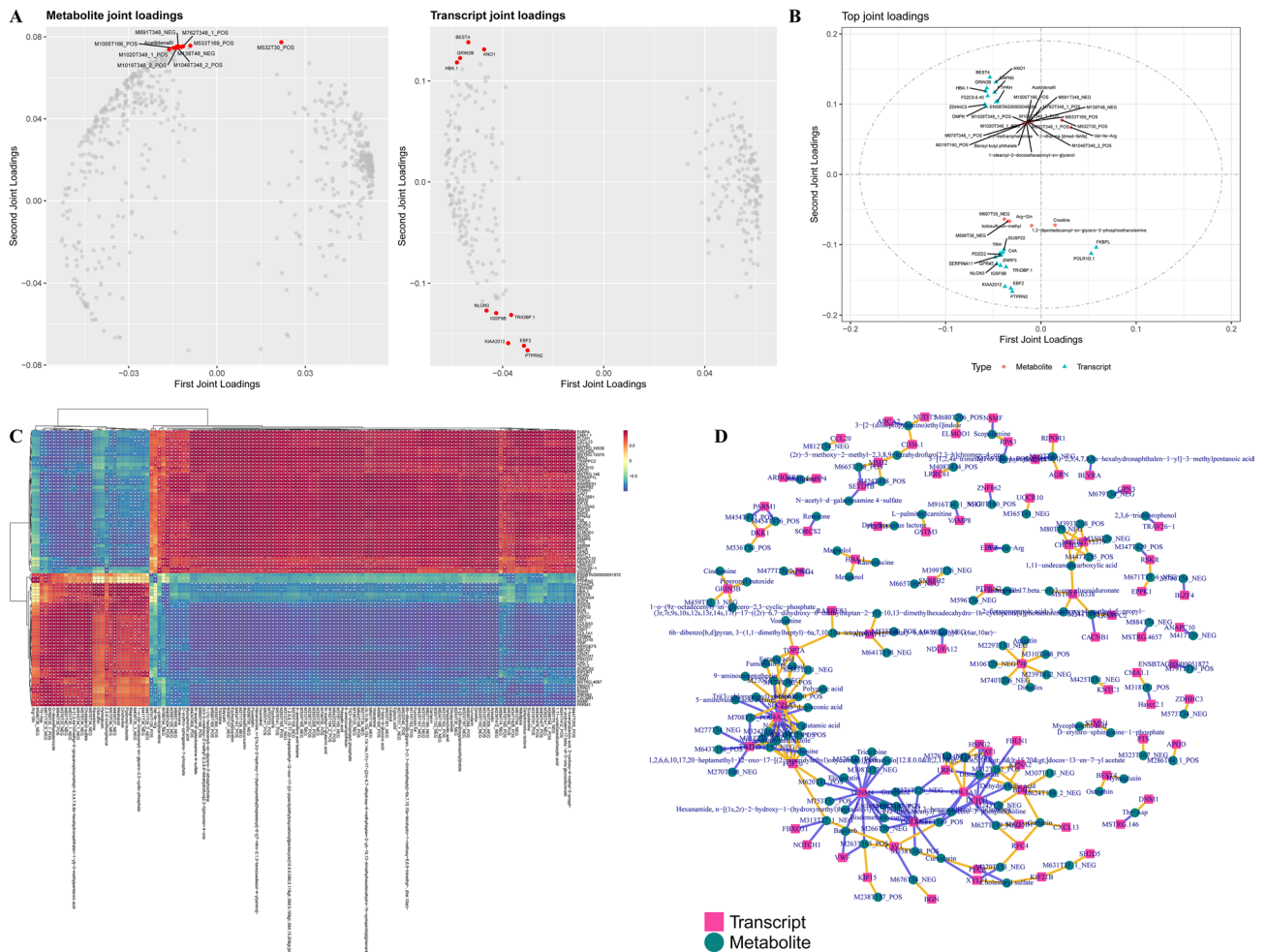


**Fig. 6** Integration of transcriptomic and metabolomic data. **(A)** The O2PLS loading plot depicts metabolomic and transcriptomic data on the left and right sides, respectively. Each data point corresponds to an individual gene or metabolite, with the horizontal and vertical axes representing the first and second dimensions of the joint section, respectively; **(B)** The loading diagram highlights the top 25 genes and metabolites with the highest squared loading values in the first two dimensions of the analysis. The selected variables were used to create loading plots, emphasizing the most strongly associated elements; **(C)** The heatmap depicts the correlation between gene expression and metabolite abundance. The heatmap displays the correlation among the top 250 differentially expressed genes and metabolites, ranked by correlation coefficient. **(D)** Correlation analysis of DEGs and DEMs. Yellow lines signify positive correlations, while blue lines indicate negative correlations. The network diagram was constructed using differentially expressed gene and metabolite data with absolute correlation coefficients exceeding 0.5, and ranked within the top 250, based on the correlation coefficient

the lipid metabolite behenic acid and transcriptionally regulated by *EBF2* (Fig. 7B). Temporal expression profiling confirmed *FABP4*'s progressive upregulation during IMAs differentiation, with significant increases observed at days 2, 4, and 6 (Fig. 7C;  $P < 0.01$ ). These integrative analyses establish *FABP4* as a pivotal mediator of vitamin A-driven adipogenesis in bovine.

**Vitamin a mediates FABP4 to positive regulate the formation of IMF**

This study synthesized siRNA (*FABP4*-118, *FABP4*-405, and *FABP4*-254) targeting *FABP4* to investigate the mechanism by which RA-regulated *FABP4* influences IMF production. Subsequently, *FABP4*-405, the most

effective siRNA for bovine *FABP4* in terms of interference efficiency, was employed in further functional studies (Fig. S3). Finding from RT-qPCR and WB analyses indicated a significant reduction in *FABP4* in IMAs following interference, while a substantial increase in *FABP4* expression was observed following the addition of RA ( $P < 0.01$ , Fig. 8A and L, Fig. S1). Lipid droplets staining revealed a significant reduction in lipid droplet accumulation in si-*FABP4* IMAs compared to the NC group, whereas RA treatment in si-*FABP4* IMAs reinstated lipid droplet accumulation (Fig. 8B-H). TG quantification confirmed this phenotype, showing 57.76% lipid depletion in *FABP4*-knockdown cells ( $P < 0.01$  vs. NC) that was recovered to the basic level after RA intervention

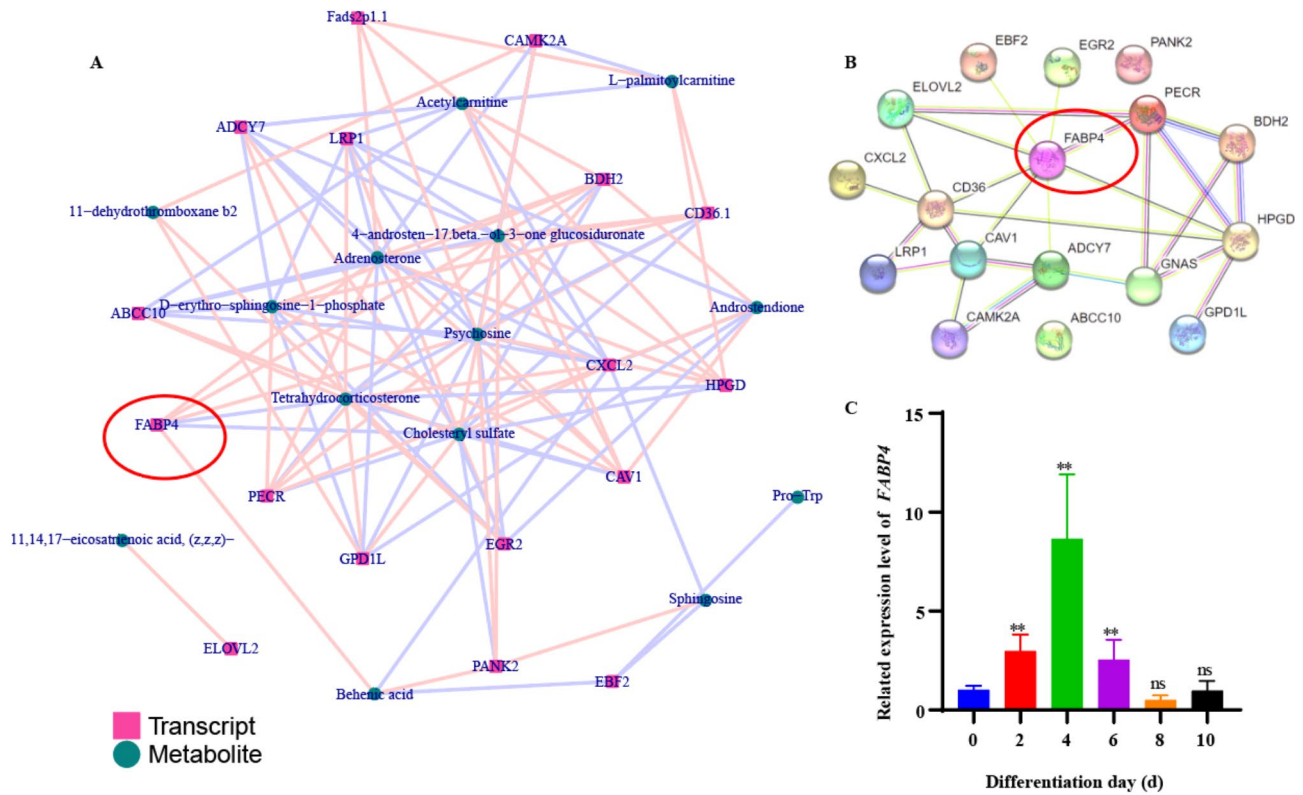


**Fig. 7** FABP4 may be the key target of vitamin A regulating bovine lipogenesis. **(A)** Interaction network analysis of DEGs and DEMs associated with lipid synthesis. The correlation analysis is carried out on the target DEGs and DEMs. Taking the absolute value of correlation  $\geq 0.8$  and  $p \leq 0.05$  as thresholds, the highly correlated substances were further screened. Red signifies a positive correlation, whereas blue signifies a negative correlation; **(B)** Examination of DEGs association networks linked to lipogenesis; **(C)** The mRNA expression level of *FABP4* in IMAs measured at different differentiation stages (0, 2, 4, 6, 8, and 10 days)

(Fig. 8I). The RT-qPCR analysis demonstrated a 39.0% reduction in *PPAR $\gamma$*  and 28.52% decrease in *LPL* transcript levels in *FABP4*-silenced IMAs versus controls ( $P < 0.01$ ; Fig. 8J-K). RA intervention not only reversed transcriptional suppression but elevated *PPAR $\gamma$* /*LPL* expression to supraphysiological levels (1.58-fold and 1.67-fold above baseline, respectively;  $P < 0.01$ ). The WB quantification corroborated these findings, demonstrating parallel depletion (49.07% reduction) and subsequent RA-induced recovery of *PPAR $\gamma$*  protein abundance ( $P < 0.01$ ; Fig. 8L, Fig. S1). These findings establish that vitamin A governs bovine IMF deposition via RA-dependent modulation of the *FABP4* signaling axis (Fig. 9).

### Discussion

IMF content serves as a critical determinant of meat quality [21], governed by IMAs proliferation and differentiation [22]. Notably, research indicates that vitamin A supplementation enhances IMF deposition in calves while maintaining systemic adiposity homeostasis [10]. After being ingested by the body, vitamin A is absorbed mainly in the form of retinol in the small intestine, combined with chylous particles, and enters the blood circulation through the lymphatic system [23]. A part of

retinol will be transported to the liver, where it will combine with retinol binding protein to form a complex for transportation to various parts of the body [23]. Retinol is first oxidized to retinol aldehyde by retinol oxidase in cells [24, 25]. It is further catalyzed by retinaldehyde dehydrogenase to form RA [24]. The process is irreversible. As an active form of vitamin A, RA regulates gene expression by combining with its receptors RAR and RXR, thus affecting the growth and differentiation of cells and maintaining the normal function of tissues [26]. Elucidating the role of RA in regulating fat formation in cattle and its underlying molecular mechanisms is crucial for improving meat quality.

Existing investigations of vitamin A-mediated lipogenesis regulation have predominantly examined two paradigms: systemic administration of retinoids to modulate fat deposition *in vivo* [10, 27], and RA-mediated adipocytes differentiation *in vitro* [10, 28, 29]. Notably, the impact of vitamin A on IMF formation and deposition differs between calves and adult cattle, with varying effects depending on dosage and developmental stage. For example, vitamin A supplementation (6,000 IU) can inhibit IMAs proliferation and marbling in adult cattle [7], while supplementation in fetal and juvenile calves

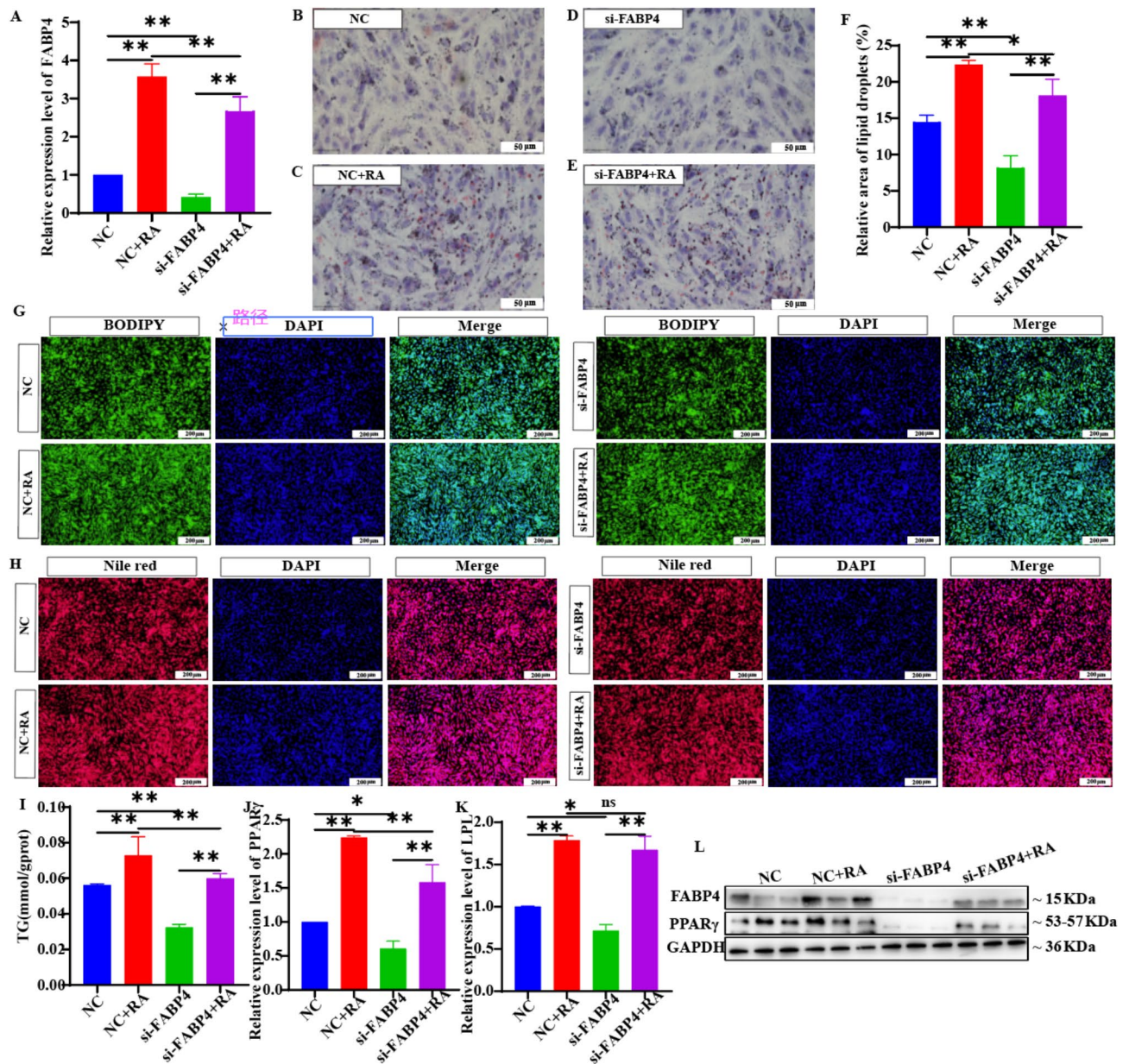


**Fig. 8** Vitamin A mediates *FABP4* to regulate the formation of IMF. **(A)** The mRNA expression levels of *FABP4* in IMAs transfected with either NC or *si-FABP4*, with or without RA treatment; **(B-E)** Oil red O staining images illustrating lipid droplets in IMAs transfected with NC or *si-FABP4*, with or without RA; **(F)** Quantitative analysis of oil red O staining intensity; **(G)** BODIPY staining images representing lipid droplets. Representative images of lipid droplets stained with Nile red; **(I)** TG content in IMAs transfected with NC and *si-FABP4*, with or without RA treatment; **(J-K)** mRNA expression of *PPAR $\gamma$*  and *LPL* in IMAs transfected with NC and *si-FABP4*, with or without RA treatment. **(M)** Protein expression of *FABP4* and *PPAR $\gamma$*  in IMAs transfected with NC or *si-FABP4*, with or without RA treatment

( $\leq 250$  days postnatal) promote IMAs proliferation [30]. Furthermore, a previous study has shown that injecting 300,000 IU vitamin A into newborn calves can increase IMF deposition by upregulating the lipogenic regulator *ZFP423*, without affecting *PPAR $\gamma$*  and *C/EBP $\alpha$*  expression [27]. A separate neonatal bovine model receiving 150,000 IU vitamin A increased the production of fat progenitor cells in skeletal muscle, accompanied by coordinated induction of *ZFP423* and *PPAR $\gamma$*  [10]. *In vitro*

research reveal RA enhances IMF formation via VEGFA/VEGFR2 signaling pathway while suppressing *PPAR $\gamma$*  and *C/EBP $\alpha$*  expression during the terminal phase of adipogenesis. Additionally, physiological concentrations of RA have been shown to have no effect on porcine IMAs differentiation [31], whereas pharmacological concentration exhibit an anti-adipogenic effect, inhibiting IMAs differentiation. The variability in experimental outcomes in previous studies may be attributed to differences in

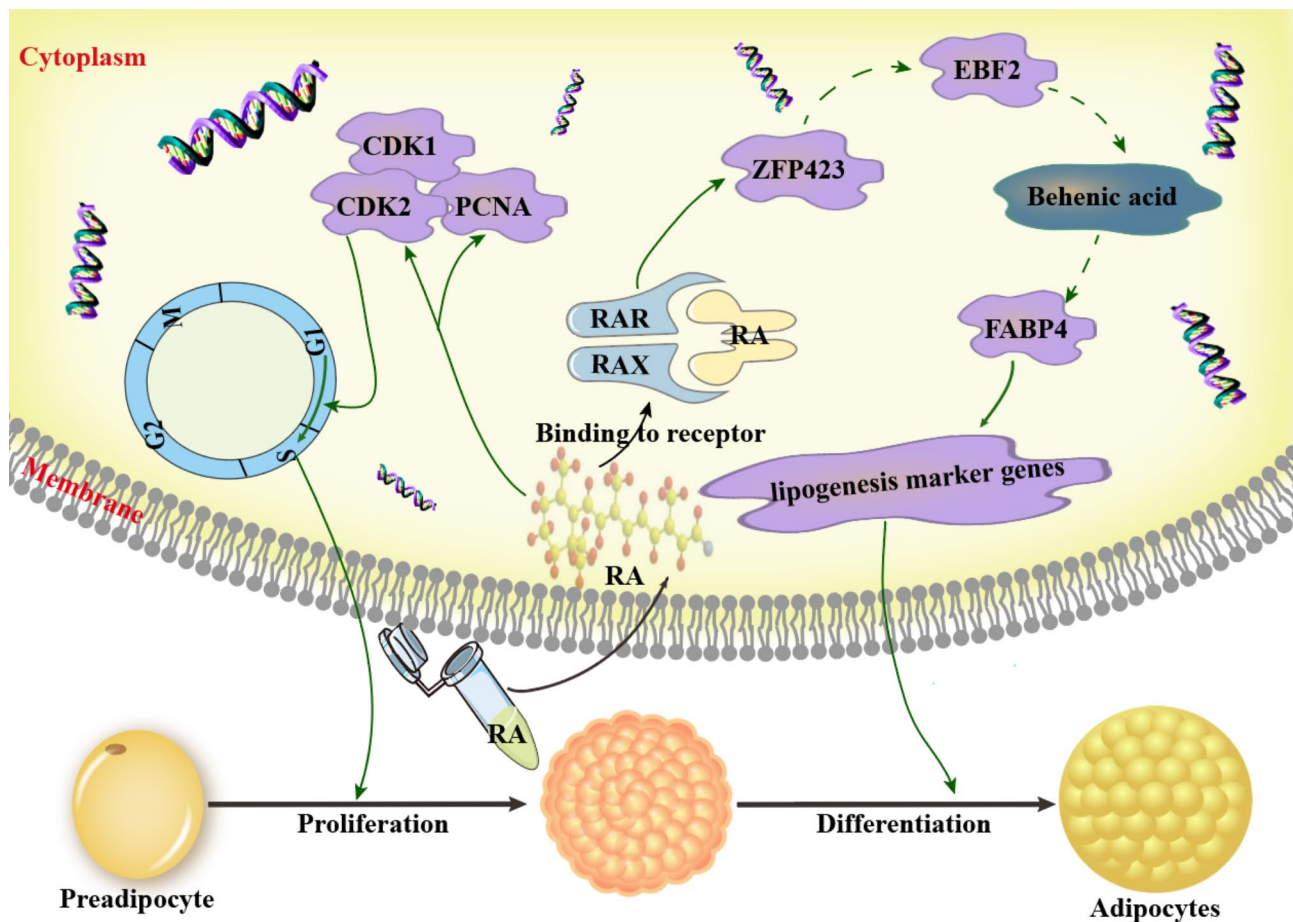


**Fig. 9** Proposed model illustrating the regulation of lipogenesis in cattle by Vitamin A through *FABP4*. Within physiological systems, vitamin A is enzymatically oxidized by alcohol dehydrogenase and aldehyde dehydrogenase to generate RA. RA binds to RAR and RXR, forming heterodimers that transcriptionally regulate *ZFP423*, a master adipogenic determinant. *ZFP423* directly governs *EBF2* expression, which in turn activates *FABP4* via behenic acid-mediated signaling cascades. *FABP4* upregulates lipid metabolism and lipogenesis markers, thereby driving IMAs differentiation. Concurrently, RA accelerates G1/S phase progression in IMAs by elevating *CDK2* and *PCNA* expression, enhancing mitotic activity. These dual regulatory axes—differentiation via *FABP4* and proliferation via *CDK2/PCNA*—collectively establish RA as a critical modulator of bovine IMF deposition. Solid lines represent established mechanisms, while dotted lines indicate potential or unknown interactions

vitamin A concentration, the stage of IMAs proliferation and differentiation, and the species of preadipocytes used. This study demonstrate that treatment with  $10^{-5}$  mol/L RA increases the proliferation and differentiation of IMAs, contributing to the existing body of knowledge and providing novel insights that could be leveraged in future mechanistic investigations.

To delineate vitamin A's molecular regulation of adipogenesis, transcriptomic and metabolomic profiling was conducted on IMAs treated with 0 or  $10^{-5}$  mol/L RA at differentiation day 6. Transcriptomic analysis identified 344 DEGs, including 18 lipogenesis-associated targets, such as *FABP4*, *CD36*, *ELOVL2*, *EBF2*, *LRP1* and *CAV1*. *FABP4* is crucial for lipogenesis regulation and lipid metabolism control [32]. It can promote adipocyte hypertrophy by binding free fatty acids, leading to increased lipid accumulation and release of free fatty acids and other fat-derived factors [33]. Its dual role in

fatty acid uptake [34] and PPAR $\gamma$ -dependent transcriptional activation underscores its necessity for adipogenesis [32, 34, 35]. *CD36*, an insulin resistance-linked receptor modulates PPAR $\gamma$ -driven lipogenesis programs [36, 37], while *ELOVL2* amplifies lipid synthesis through *FABP4* and *DEGT2* induction [38]. *EBF2*, regulated by *FABP4* and *ZFP423*, further fine-tunes PPAR $\gamma$  activity [39, 40]. Metabolomic profiling revealed RA-induced alterations in metabolites implicated in fatty acid biosynthesis, metabolism, and insulin resistance, including cholesteryl sulfate, D-erythro-sphosphorite-1-phosphate, psychosine, 4-androsten-17 $\beta$ -ol-3-one glucosiduronate and L-palmitoylcystine [41–44]. *LRP1* emerged as a dual regulator of lipolysis and PPAR $\gamma$  coactivation, modulating cholesterol homeostasis via ACC targeting and Wnt5a signal pathway [45, 46]. *CAV1*, a caveolae scaffold protein, suppressed fatty acid oxidation by enhancing SREBP1 expression [47–49]. Importantly, integrated

transcriptomic and metabolomic analyses once again confirmed the central regulatory roles of *FABP4*, *CD36*, *EBF2*, *LRP1* and *CAV1* in RA-mediated bovine adipogenesis. And, we found that *FABP4* can be directly or indirectly associated with *CD36*, *EBF2*, *LRP1* and *CAV1*, and it plays a core role in this network (Fig. 7). In addition, molecular experiments also found that RA can regulate the expression of lipogenesis markers by affecting the expression of *FABP4*, and then positively regulate the lipogenesis of cattle.

Integrated transcriptome and metabolomic analysis identified that RA-affected DEGs and metabolites were enriched in the calcium signaling pathway (ko04020), unsaturated fatty acid biosynthesis (ko04020), biosynthesis of unsaturated fatty acids (ko01040), insulin resistance (ko04931), and fatty acid metabolism (ko01212). Calcium signaling, a pivotal regulator of adipocyte differentiation and lipid metabolism [50], exerts pleiotropic effects through  $Ca^{2+}$ -dependent modulation of cellular proliferation, differentiation, and apoptosis [51, 52]. Elevated extracellular  $Ca^{2+}$  concentrations (>5 mmol/L) suppress preadipocyte differentiation [51], while dietary calcium supplementation reduces adiposity and enhances weight loss independent of caloric intake [53]. Furthermore, RA-driven perturbations in unsaturated fatty acids biosynthesis [54], insulin resistance [55], and fatty acid metabolism [56] further implicate these pathways in IMF production and deposition. This suggests that RA may significantly influence these metabolic pathways related to fatty acid biosynthesis and metabolism, contributing to its effects on IMF production.

## Conclusion

In summary, this study establishes that vitamin A potentiates IMF formation through its bioactive metabolite RA, which transcriptionally activates *FABP4* to orchestrate lipogenic marker expression, driving adipocyte differentiation and lipid droplet deposition. However, the precise molecular network formed by RA regulating IMF through *FABP4* needs to be further investigated, and these findings need to be verified at the *in vivo* level. Future research dissecting this network may reveal new molecular targets to improve cattle meat quality.

## Supplementary Information

The online version contains supplementary material available at <https://doi.org/10.1186/s12864-025-11544-7>.

Supplementary Material 1

## Author contributions

YPS, JPZ, WDW and GJZ conceived the study. YPS and JPZ drafted the manuscript. CJ, XYS, XDC, SHAR, DPS, YM, LSZ, DWW and GJZ revised the manuscript. DWW and GJZ finalized the manuscript. All authors read and approved the final manuscript.

## Funding

This research received support from the Natural Science Foundation of China (U24A20446, 32202641 & 32460819), the Key R & D projects in Ningxia Hui Autonomous Region (2021BEF02020), the Central Guidance on Local Science and Technology Development Fund (2024FRD05052), the National Science and Technology Major Project-Science and Technology Innovation 2030 (2023ZD0404803-02), and the Ningxia Ruminant Nutrition Science and Technology Innovation Team (2024CXTD008).

## Data availability

The study's data and materials can be obtained from the corresponding author upon reasonable request. The RNA-seq data generated in the current study are available in the NCBI database (<https://www.ncbi.nlm.nih.gov/bioproject/PRJNA1214066>).

## Declarations

### Ethics approval and consent to participate

Not applicable.

### Consent for publication

Not applicable.

### Competing interests

The authors declare no competing interests.

Received: 14 January 2025 / Accepted: 28 March 2025

Published online: 24 April 2025

## References

- Gonzalez N, Marques M, Nadal M, Domingo JL. Meat consumption: which are the current global risks? A review of recent (2010–2020) evidences. *Food Res Int* 2020, 137.
- Hossain MAM, Uddin SMK, Sultana S, Wahab YA, Sagadevan S, Johan MR, Ali ME. Authentication of Halal and kosher meat and meat products: analytical approaches, current progresses and future prospects. *Crit Rev Food Sci Nutr*. 2022;62(2):285–310.
- He S, Yu D, Li P, Zhang M, Xing S, Liu B, Sun C, Liu L, Li Z-H. A new perspective on endocrine disrupting effects of Triphenyltin on marine Medaka: from brain transcriptome, gut content metabolome and behavior. *Chemosphere* 2022, 307.
- Peng DQ, Smith SB, Lee HG. Vitamin A regulates intramuscular adipose tissue and muscle development: promoting high-quality beef production. *J Anim Sci Biotechnol* 2021, 12(1).
- Rosen ED, Spiegelman BM. What we talk about when we talk about fat. *Cell*. 2014;156(1–2):20–44.
- Ghaben AL, Scherer PE. Adipogenesis and metabolic health. *Nat Rev Mol Cell Biol*. 2019;20(4):242–58.
- Kruk ZA, Bottema MJ, Reyes-Veliz L, Forder REA, Pitchford WS, Bottema CDK. Vitamin A and marbling attributes: intramuscular fat hyperplasia effects in cattle. *Meat Sci*. 2018;137:139–46.
- Oka A, Maruo Y, Miki T, Yamasaki T, Saito T. Influence of vitamin A on the quality of beef from the Tajima strain of Japanese black cattle. *Meat Sci*. 1998;48(1–2):159–67.
- Harris CL, Wang B, Deavila JM, Busboom JR, Maquiver M, Parish SM, McCann B, Nelson ML, Du M. Vitamin A administration at birth promotes calf growth and intramuscular fat development in Angus beef cattle. *J Anim Sci Biotechnol* 2018, 9.
- Yu X, Ma Y, Luo Y, Tang G, Jiang Z, Zhang J, Ye B, Huang Z, Luo Y, Du M et al. Neonatal vitamin A administration increases intramuscular fat by promoting angiogenesis and preadipocyte formation. *Meat Sci* 2022, 191.
- Li W, Wang F, Sun F, Qu Y, Liu C, Han Y, Wang H, Jiang B, Zhong P, Wang J et al. Effects of vitamin A on intramuscular fat development in beef cattle: A meta-analysis. *Front Veterinary Sci* 2023, 10.
- VanBuren CA, Everts HB. Vitamin A in skin and hair: an update. *Nutrients* 2022, 14(14).
- Krone KG, Ward AK, Madder KM, Hendrick S, McKinnon JJ, Buchanan FC. Interaction of vitamin A supplementation level with ADH1C genotype on intramuscular fat in beef steers. *Animal*. 2016;10(3):403–9.

14. Chen G. Roles of vitamin A metabolism in the development of hepatic insulin resistance. *ISRN Hepatol*. 2013;2013:534972–534972.
15. Schwarz EJ, Reginato MJ, Shao D, Krakow SL, Lazar MA. Retinoic acid blocks adipogenesis by inhibiting C/EBP $\beta$ -mediated transcription. *Mol Cell Biol*. 1997;17(3):1552–61.
16. Kim DM, Choi H-R, Park A, Shin S-M, Bae K-H, Lee SC, Kim I-C, Kim WK. Retinoic acid inhibits adipogenesis via activation of Wnt signaling pathway in 3T3-L1 preadipocytes. *Biochem Biophys Res Commun*. 2013;434(3):455–9.
17. Chen F-F, Xiong Y, Peng Y, Gao Y, Qin J, Chu G-Y, Pang W-J, Yang G-S. miR-425-5p inhibits differentiation and proliferation in Porcine intramuscular preadipocytes. *Int J Mol Sci* 2017, 18(10).
18. Song Y, Zhang J, Jiang C, Song X, Wu H, Zhang J, Raza SHA, Zhang L, Zhang L, Cai B et al. FOXO1 regulates the formation of bovine fat by targeting CD36 and STEAP4. *Int J Biol Macromol* 2023, 248.
19. Nie X, Dong X, Hu Y, Xu F, Hu C, Shu C. Coenzyme Q10 stimulate reproductive vitality. *Drug Des Dev Therapy*. 2023;17:2623–37.
20. Livak KJ, Schmittgen TD. Analysis of relative gene expression data using real-time quantitative PCR and the 2- $\Delta\Delta$ CT method. *Methods*. 2001;25(4):402–8.
21. Guo H, Khan R, Raza SHA, Ning Y, Wei D, Wu S, Hosseini SM, Ullah I, Garcia MD, Zan L. KLF15 promotes transcription of KLF3 gene in bovine adipocytes. *Gene*. 2018;659:77–83.
22. Du M, Tong J, Zhao J, Underwood KR, Zhu M, Ford SP, Nathanielsz PW. Fetal programming of skeletal muscle development in ruminant animals. *J Anim Sci*. 2010;88:E51–60.
23. Dikun KM, Gudas LJ. Vitamin A and retinoid signaling in the kidneys. *Pharmacol Ther* 2023, 248.
24. Blaner WS. Vitamin A signaling and homeostasis in obesity, diabetes, and metabolic disorders. *Pharmacol Ther*. 2019;197:153–78.
25. Milosheska D, Roskar R. Use of retinoids in topical antiaging treatments: A focused review of clinical evidence for conventional and nanoformulations. *Adv Therapy*. 2022;39(12):5351–75.
26. Mody N. Alterations in vitamin A/retinoic acid homeostasis in diet-induced obesity and insulin resistance. *Proc Nutr Soc*. 2017;76(4):597–602.
27. Maciel FC, Machado Neto OR, Duarte MS, Du M, Lage JF, Teixeira PD, Martins CL, Domingues EHR, Fogaca LA, Ladeira MM. Effect of vitamin A injection at birth on intramuscular fat development and meat quality in beef cattle. *Meat Sci* 2022, 184.
28. Berry DC, Soltanian H, Noy N. Repression of cellular retinoic Acid-binding protein II during adipocyte differentiation. *J Biol Chem*. 2010;285(20):15324–32.
29. Berry DC, DeSantis D, Soltanian H, Croniger CM, Noy N. Retinoic acid upregulates preadipocyte genes to block adipogenesis and suppress Diet-Induced obesity. *Diabetes*. 2012;61(5):1112–21.
30. Wang B, Yang Q, Harris CL, Nelson ML, Busboom JR, Zhu M-J, Du M. Nutrigenomic regulation of adipose tissue development - role of retinoic acid: A review. *Meat Sci*. 2016;120:100–6.
31. Suryawan A, Hu CY. Effect of retinoic acid on differentiation of cultured pig preadipocytes. *J Anim Sci*. 1997;75(1):112–7.
32. Trojnar M, Patro-Malysza J, Kimber-Trojnar Z, Leszczynska-Gorzela B, Mosiewicz J. Associations between Fatty Acid-Binding Protein 4-A Proinflammatory Adipokine and Insulin Resistance, Gestational and Type 2 Diabetes Mellitus. *Cells* 2019, 8(3).
33. Chung JY, Hong J, Kim H-J, Song Y, Yong S-B, Lee J, Kim Y-H. White adipocyte-targeted dual gene Silencing of FABP4/5 for anti-obesity, anti-inflammation and reversal of insulin resistance: efficacy and comparison of administration routes. *Biomaterials* 2021, 279.
34. Hotamisligil GS, Bernlohr DA. Metabolic functions of FABPs—mechanisms and therapeutic implications. *Nat Reviews Endocrinol*. 2015;11(10):592–605.
35. Berger E, Geloan A. FABP4 controls fat mass expandability (Adipocyte size and Number) through Inhibition of CD36/SR-B2 signalling. *Int J Mol Sci* 2023, 24(2).
36. Yang J, Park KW, Cho S. Inhibition of the CD36 receptor reduces visceral fat accumulation and improves insulin resistance in obese mice carrying the BDNF-Val66Met variant. *J Biol Chem*. 2018;293(34):13338–48.
37. Su T, Huang C, Yang C, Jiang T, Su J, Chen M, Fatima S, Gong R-H, Hu X, Bian Z et al. vol 152, 104586;: Apigenin inhibits STAT3/CD36 signaling axis and reduces visceral obesity (2020). *Pharmacological Research* 2023, 193.
38. Kobayashi T, Zadavec D, Jacobsson A. ELOVL2 overexpression enhances triacylglycerol synthesis in 3T3-L1 and F442A cells. *FEBS Lett*. 2007;581(17):3157–63.
39. Stine RR, Shapira SN, Lim H-W, Ishibashi J, Harms M, Won K-J, Seale P. EBF2 promotes the recruitment of beige adipocytes in white adipose tissue. *Mol Metabolism*. 2016;5(1):57–65.
40. Shao M, Zhang Q, Truong A, Shan B, Vishvanath L, Li L, Seale P, Gupta RK. ZFP423 controls EBF2 coactivator recruitment and PPAR $\gamma$  occupancy to determine the thermogenic plasticity of adipocytes. *Genes Dev*. 2021;35(21–22):1461–74.
41. Xu D, Ma R, Ju Y, Song X, Niu B, Hong W, Wang R, Yang Q, Zhao Z, Zhang Y et al. Cholesterol sulfate alleviates ulcerative colitis by promoting cholesterol biosynthesis in colonic epithelial cells. *Nat Commun* 2022, 13(1).
42. Takashiro Y, Nakamura H, Koide Y, Nishida A, Murayama T. Involvement of p38 MAP kinase-mediated cytochrome release on sphingosine-1-phosphate (S1P)- and monomethyl-S1P-induced cell death of PC12 cells. *Biochem Pharmacol*. 2005;70(2):258–65.
43. Kanazawa T, Nakamura S, Momoi M, Yamaji T, Takematsu H, Yano H, Sabe H, Yamamoto A, Kawasaki T, Kozutsumi Y. Inhibition of cytokinesis by a lipid metabolite, psychosine. *J Cell Biol*. 2000;149(4):943–50.
44. Haruna T, Horie M, Takano M, Kono Y, Yoshida H, Otani H, Kubota T, Ninomiya T, Akao M, Sasayama S. Alteration of the membrane lipid environment by L-palmitoylcarnitine modulates K<sup>+</sup> (ATP) channels in guinea-pig ventricular myocytes. *Pflügers Archiv-European J Physiol*. 2000;441(2–3):200–7.
45. Terrand J, Bruban V, Zhou L, Gong W, El Asmar Z, May P, Zurhove K, Haffner P, Philippe C, Woltd E, et al. LRP1 controls intracellular cholesterol storage and fatty acid synthesis through modulation of Wnt signaling. *J Biol Chem*. 2009;284(1):381–8.
46. Mao H, Lockyer P, Li L, Ballantyne CM, Patterson C, Xie L, Pi X. Endothelial LRP1 regulates metabolic responses by acting as a co-activator of PPAR $\gamma$ . *Nat Commun* 2017, 8.
47. Zhang Q, Wang J, Li H, Zhang Y, Chu X, Yang J, Li Y. LncRNA Gm12664-001 ameliorates nonalcoholic fatty liver through modulating miR-295-5p and CAV1 expression. *Nutr Metabolism* 2020, 17(1).
48. Wang J, Jiang W, Xin J, Xue W, Shi C, Wen J, Huang Y, Hu C. Caveolin-1 alleviates Acetaminophen-Induced fat accumulation in Non-Alcoholic fatty liver disease by enhancing hepatic antioxidant ability activating AMPK pathway. *Front Pharmacol* 2021, 12.
49. Ma APY, Yeung CLS, Tey SK, Mao X, Wong SWK, Ng TH, Ko FCF, Kwong EML, Tang AHN, Ng IO-L, et al. Suppression of ACADM-Mediated fatty acid oxidation promotes hepatocellular carcinoma via aberrant CAV1/SREBP1 signaling. *Cancer Res*. 2021;81(13):3679–92.
50. Sun C, Qi R, Wang L, Yan J, Wang Y. p38 MAPK regulates calcium signal-mediated lipid accumulation through changing VDR expression in primary preadipocytes of mice. *Mol Biol Rep*. 2012;39(3):3179–84.
51. Jensen B, Farach-Carson MC, Kenaley E, Akanbi KA. High extracellular calcium attenuates adipogenesis in 3T3-L1 preadipocytes. *Exp Cell Res*. 2004;301(2):280–92.
52. Soliman EM, Rodrigues MA, Gomes DA, Sheung N, Yu J, Amaya MJ, Nathanson MH, Dranoff JA. Intracellular calcium signals regulate growth of hepatic stellate cells via specific effects on cell cycle progression. *Cell Calcium*. 2009;45(3):284–92.
53. Parra P, Bruni G, Palou A, Serra F. Dietary calcium Attenuation of body fat gain during high-fat feeding in mice. *J Nutr Biochem*. 2008;19(2):109–17.
54. Li W, Qiu L, Guan J, Sun Y, Zhao J, Du M. Comparative transcriptome analysis of longissimus dorsi tissues with different intramuscular fat contents from Guangling donkeys. *BMC Genomics* 2022, 23(1).
55. Park S, Yoo KM, Hyun JS, Kang S. Intermittent fasting reduces body fat but exacerbates hepatic insulin resistance in young rats regardless of high protein and fat diets. *J Nutr Biochem*. 2017;40:14–22.
56. Chen J, You R, Lv Y, Liu H, Yang G. Conjugated Linoleic acid regulates adipocyte fatty acid binding protein expression peroxisome proliferator-activated receptor a signaling pathway and increases intramuscular fat content. *Front Nutr* 2022, 9.

## Publisher's note

Springer Nature remains neutral with regard to jurisdictional claims in published maps and institutional affiliations.